

LETTER • **OPEN ACCESS**

## Ultrafast X-ray laser-induced explosion: How the depth influences the direction of the ion trajectory







To cite this article: Emiliano De Santis *et al* 2024 *EPL* **148** 17001

View the [article online](#) for updates and enhancements.

You may also like

- [Review of soft x-ray laser researches and developments](#)  
Hiroyuki Daido
- [Hot and dense plasma probing by soft X-ray lasers](#)  
M. Krs, M. Kozlová, J. Nejdil et al.
- [Impact of discharge current profile on the lasing efficiency of 46.9 nm capillary discharge soft x-ray laser](#)  
S Barnwal, S Nigam, K Aneesh et al.

# Ultrafast X-ray laser-induced explosion: How the depth influences the direction of the ion trajectory

EMILIANO DE SANTIS<sup>1,2,3(a)</sup> , IBRAHIM DAWOD<sup>2,4</sup> , TOMAS ANDRÉ<sup>2</sup> , SEBASTIAN CARDOCH<sup>2</sup> ,  
NICUSOR TIMNEANU<sup>2</sup>  and CARL CALEMAN<sup>2,5(b)</sup> 

<sup>1</sup> Department of Chemistry – BMC, Uppsala University - Box 576, SE-751 23 Uppsala, Sweden

<sup>2</sup> Department of Physics and Astronomy, Uppsala University - Box 516, SE-751 20 Uppsala, Sweden

<sup>3</sup> Department of Physics and INFN, University of Rome Tor Vergata - I-00133 Rome, Italy

<sup>4</sup> European XFEL - Holzkoppel 4, DE-22869 Schenefeld, Germany

<sup>5</sup> Center for Free-Electron Laser Science CFEL, Deutsches Elektronen-Synchrotron DESY - Notkestraße 85, DE-22607 Hamburg, Germany

received 28 February 2024; accepted in final form 9 September 2024  
published online 10 October 2024

**Abstract** – Single particle imaging using X-ray lasers is a technique aiming to capture atomic resolution structures of biomolecules in their native state. Knowing the particle’s orientation during exposure is crucial for method enhancement. It has been shown that the trajectories of sulfur atoms in a Coulomb exploding lysozyme are reproducible, providing orientation information. This study explores if sulfur atom depth influences explosion trajectory. Employing a hybrid collisional-radiative/molecular dynamics model, we analyze the X-ray laser-induced dynamics of a single sulfur ion at varying depths in water. Our findings indicate that the ion spread-depth relationship depends on pulse parameters. At a photon energy of 2 keV, high-charge states are obtained, resulting in an increase of the spread with depth. However, at 8 keV photon energy, where lower charge states are obtained, the spread is essentially independent with depth. Finally, lower ion mass results in less reproducible trajectories, opening a promising route for determining protein orientation through the introduction of heavy atoms.



Copyright © 2024 The author(s)

Published by the EPLA under the terms of the [Creative Commons Attribution 4.0 International License](https://creativecommons.org/licenses/by/4.0/) (CC BY). Further distribution of this work must maintain attribution to the author(s) and the published article’s title, journal citation, and DOI.

**Introduction.** – From the time when large-scale X-ray facilities such as synchrotrons were first introduced, they have been the workhorse for the determination of the molecular structure of biological macromolecules such as proteins. X-ray crystallography has an outstanding position as the most used technique to determine protein structures. To date, a vast majority of all proteins structures listed in the Protein Data Base [1] have been characterized using X-ray crystallography. Photons in the X-ray regime used in diffractive imaging will induce photoionization in the molecule, which in turn destroys the structure —either directly, or indirectly by secondary ionization cascades or via the creation of radicals. In crystallography,

such radiation damage can to some extent be ignored since it will be spread out over multiple copies of the protein in the crystal. But when the damage gets too high and structural changes occur, the protein crystal stops to diffract into the Bragg spots and the crystal “dies” [2].

Another X-ray technique to determine biomolecular structures is the so-called Single Particle Imaging (SPI) using X-ray Free-electron Lasers (XFELs) [3]. This more recent method employs an intense XFEL pulse to capture images of individual protein molecules, unlike crystallography, which relies on a crystal lattice. However, this ultra-intense photon beam severely damages the molecules, leading to their destruction during the process. The principle behind SPI is that one needs to repeat the experiment numerous (millions of) times to accumulate sufficient data for analysis [4]. The unknown orientation of the particle at the time it is hit by the beam renders its 3D reconstruction

<sup>(a)</sup>E-mail: [emiliano.desantis@physics.uu.se](mailto:emiliano.desantis@physics.uu.se) (corresponding author)

<sup>(b)</sup>E-mail: [carl.caleman@physics.uu.se](mailto:carl.caleman@physics.uu.se)

problematic, complicated, and resource-intensive in terms of significant sample consumption and required beamtime. Presently, data processing solely relies on information from diffraction patterns, requiring sorting and clustering of all diffraction images [5,6]. Capturing additional information about the protein orientation concurrently with coherent scattering would significantly benefit algorithms to correlate diffraction images [7,8].

One potential approach to obtain such information *a priori* involves protein manipulation, such as employing external electric fields [7,9,10] or utilizing flow alignment techniques [11]. Conversely, an alternative strategy to determine the orientation of the protein *a posteriori* is to take advantage of the unavoidable radiation damage by measuring the directions of the ejected ions from the Coulomb explosion of the protein. In a computational study [12], it has been shown how the sulfur atoms from a lysozyme protein, triggered by their interaction with the FEL X-rays beam, tend to follow similar trajectories across 150 independent simulations. Sulfur atoms belonging to cysteine residues in disulfide bonds exhibited a narrower spread compared to those from methionine residues, which showed more variability in their trajectories. The choice to examine sulfur atoms is given by their widespread presence in nearly all proteins, as observed in 95% of the 78742 biological protein structures we retrieved from the Protein Data Bank in Europe [13]. Despite their occurrence in such a high percentage of proteins, sulfur atoms constitute only about 0.4% of the atoms within these. Owing to the rarity of these atomic species within the molecular composition, the analysis of sulfur explosion trajectories could therefore serve as a unique and distinctive identifier specific to the studied protein. Since lysozyme is a rather small protein, and most of the sulfurs are close to its surface, it is hard to draw any conclusions of how well defined the trajectories of atoms heavier than N, C or O from a larger protein would be. To validate if the findings from the simulations hold in an experimental setting, it is necessary to design an experiment to test this. In such an experiment, it is essential to know how the distance from the surface of the protein affects the direction of the ion path. In the present study, we address this question by placing a single sulfur atom at different distances from a water surface. By mimicking the scenario where sulfur atoms are in methionine residues, representing the worst-case scenario of the aforementioned study, and measuring the spread of its trajectory on a detector placed at a given distance from the water surface, we investigate how close to the surface of a biomolecule an atom can be to possibly provide reliable orientation information. In our simulation setup we have decided to use water as the bulk material, instead of a protein. The reason for this is that we expect that it is experimentally easier to place a sulfur ion at different distances from a water surface, and we expect water to exhibit less structural complexity compared to a protein. Moreover, given the high intensity of the FEL beam, protein bonds would likely break

in the early simulation steps, resulting in an environment for the sulfur atom that closely resembles the environment experienced by sulfur in water under the same FEL beam conditions. Consequently, the spread observed in the ion ejected from a water bulk is not expected to overestimate that of an ion ejected from a more structured protein environment.

## Methods. –

*Hybrid CR/MD simulations.* Building on earlier work [12,14–16], we have used an updated hybrid model, MOLDSTRUCT [17], that combines collisional-radiative (CR) simulations with classical molecular dynamics (MD) to study photon-matter interaction and atomic dynamics. Given a sample’s stoichiometry and density and X-ray’s pulse shape, duration, energy bandwidth, photon energy and focus, we computed the time-evolution of the atomic charge states, free electron density and free electron temperature with CR code CRETIN [18,19]. We used this information together with an atomic structure model and force field to carry out MD simulations with an in-house development version of GROMACS [20]. At each MD time step, the charge distribution of each atomic species is applied and the parameters of the Coulomb potential are calculated. The interaction between the atoms is formulated using pair potentials. For the non-bonded interactions, a hybrid Coulomb screening potential is utilized, which is based on a combination of the ion-sphere and the Debye screening potential active at different intervals [21] such that

$$\begin{aligned}\phi(r) &= \phi_{\text{ion-sphere}}(r)\Big|_0^{r'} + \phi_{\text{Debye}}(r)\Big|_{r'}^r \\ &= \frac{c_0}{r} + c_1 - c_2 r^2 + \frac{c_3}{r} \exp\left(-\frac{r}{\lambda_D}\right).\end{aligned}\quad (1)$$

The constants  $c_0$ ,  $c_1$ ,  $c_2$  and  $c_3$  can be computed from certain imposed boundary conditions, and  $r'$  is the transition point between the two models calculated by

$$r' = \lambda_D \left[ \left( \left( \frac{R}{\lambda_D} \right)^3 + 1 \right)^{1/3} - 1 \right], \quad (2)$$

where  $R$  is the ion-sphere radius that for an ion with charge  $Q$ , and free electron density  $n_e$  is defined as

$$R = \left( \frac{3Q}{4\pi n_e} \right)^{1/3}. \quad (3)$$

The Debye length  $\lambda_D$  defined as

$$\lambda_D = \sqrt{\frac{\epsilon_0 k_B T_e}{n_e e^2}}, \quad (4)$$

where  $\epsilon_0$  is the permittivity of free space,  $T_e$  the electron temperature,  $e$  is the elementary charge, and  $k_B$  the Boltzmann constant.

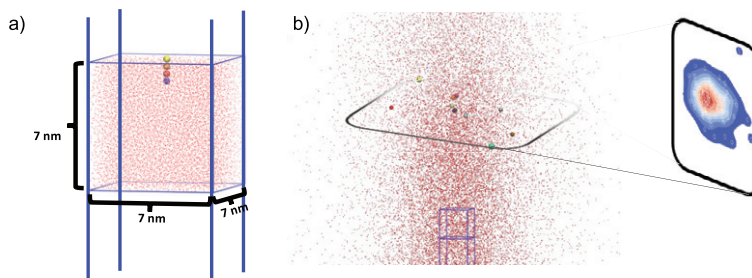


Fig. 1: Panel (a): visualization of the initial setup preceding simulation. For each system, the sulfur atom is placed at varying distances from the surface of the bulk water. Panel (b): illustration of the system subsequent to interaction with the X-ray beam. The positions of sulfur atoms are projected onto a plane perpendicular to the water surface, enabling the evaluation of their distribution density.

We initially modelled non-bonded interactions with a Lennard-Jones (LJ) potential, but the simulations suffered from numerical instabilities. We instead opted to model only the repulsive part of the van der Waals interaction using a Morse potential [22], that for pairs of atoms  $i$  and  $j$ , has the form

$$V_{\text{van der Waals}}(r_{ij}) = D_{ij}(1 - \exp(-\beta_{ij}(r_{ij} - b_{ij})))^2, \quad (5)$$

where  $D_{ij}$  is the dissociation energy,  $b_{ij}$  the equilibrium distance, and  $r_{ij}$  the interatomic distance. For distances larger than the equilibrium distance,  $r \geq b_{ij}$ , the potential was set to zero. To incorporate ionization effects, the steepness parameter  $\beta_{ij}$  was scaled by a coefficient  $c_{i,j} = 1/2([1 - q_i/Z_i] + [1 - q_j/Z_j])$ , where  $q$  and  $Z$  are the charge and atomic number of atoms  $i$  and  $j$ . As the pairs of atoms ionize, the range and magnitude of the electron cloud decreases. The scaling parameter, therefore, reduces the repulsive interaction and allows atoms to come closer. We also modelled bonded interactions with a Morse potential [22] since the force always converges to zero for large distances, mimicking bond breaking.

Validating these models against experimental data is not a straightforward task. However, in an earlier study, we compared the expected diffracted signal from a water jet based on our theoretical framework, to the experimentally recorded diffraction pattern [14]. This comparison revealed a strong agreement, strengthening our confidence in the model's validity. Furthermore, this hybrid/MD approach to study photon-matter interaction at XFELs has proven to reproduce other experimental findings [23,24].

In order to generate initial structures to perform the MD simulations and to capture enough statistics, a 100 ps long equilibrated bulk simulation of a cubic water box of 7 nm of side is performed. The temperature is kept constant (and equal to 300 K) by using the velocity rescaling thermostat [25] with a 0.1 ps coupling time. Pressure is kept constant at 1 bar by using the Berendsen barostat [26] with a 1 ps coupling time and an isothermal compressibility of  $4.5 \times 10^5 \text{ bar}^{-1}$ . For both the equilibrium and the CR/MD simulations, the TIP3P model is used given by the CHARMM force field [27,28]. Periodic boundary

conditions (PBC) are imposed to the system, and the Particle Mesh Ewald algorithm is employed for dealing with the long-range Coulomb interactions [29]. Newton's equations were solved by using a time step of 2 fs. A non-bonded pair list with a 1.4 nm cut-off is updated every 10 steps.

From the bulk simulations, frames every 1 ps were extracted. For each of them, the side of the box in the  $z$ -direction was expanded, ending up with the introduction of water-vacuum interface. Thereafter, a sulfur ion was placed at different depths  $D$  ( $D \in [0, 1, 2, 3, 4, 6, 8, 10, 12, 14]$  Å) from the water-vacuum interface by replacing water molecules lying within  $2.5$  Å from  $D$  and at the center of the  $xy$  plane. Structures undergo energy minimization followed by 250 fs equilibration in the NVE ensemble. In this last stage, the sulfur coordinates are kept fixed and the water molecules can rearrange freely around it. A schematic representation of the simulation setup is given in panel a of fig. 1.

Two sets of pulse parameters were used. For the soft X-ray range, we utilized a photon energy of 2 keV and an intensity of  $10^{18} \text{ Wcm}^{-2}$ . In the second case, hard X-rays were used with a photon energy of 8 keV and an intensity of  $6 \times 10^{18} \text{ Wcm}^{-2}$ . For both pulses, a duration of 15 fs was used. The photon parameters are similar to those achievable at XFEL sources [14]. PBC were imposed to the system in the  $x$ - and  $y$ -direction, however not in the  $z$ -direction, thus allowing for expansion in this dimension. The integration time step was set to  $10^{-5}$  ps. Long range electrostatic interactions were calculated using a cut-off scheme. The value was determined based on the distance where the largest Coulomb forces computed from the CR data was small. Trajectories as long as 500 fs were collected. A total of 100 independent simulations are performed for any choice of the pulse parameters and ion depth.

*Analysis.* Trajectories are analysed as follows. First of all, the periodic boundary condition of the system were treated ensuring uninterrupted paths for the atoms. Subsequently, for each independent simulation, once the sulfur atom traveled a distance of 65 Å from the water surface

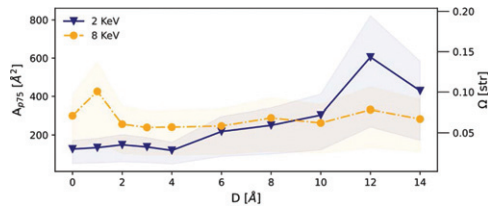


Fig. 2: Results of the sulfur atoms’ explosion behavior are shown as a function of their depth at the beginning of the simulations. Projections of ion positions onto a plane, situated parallel to and at a specified distance of 65 Å from the water surface, were evaluated using kernel density estimation. The areas covered by the 75th percentiles of the point distribution are displayed. Results of explosions induced by 2 keV photo energies are depicted in orange, while those corresponding to 8 keV are shown in blue. The second  $y$ -axis in the plot indicates the respective solid angles spanned by the point distributions. The shaded regions represent the areas covered by the 90th and 66th percentiles for the respective energy levels, defining the range of variation around the central tendency.

in the  $z$ -direction, its coordinates were projected onto a plane parallel to it. This analysis emulates the concept of a detector positioned at a specific distance from the sample. To quantify the distribution’s extent, we eventually make use of kernel density estimator from seaborn python library [30] (see panel (b) of fig. 1) and calculate the area encompassing various percentiles of the point distribution using the Shoelace formula [31]. However, due to the consistency in the results across the different percentiles, we exclusively present data for the 75th percentile in the subsequent sections. Although hydrogens are explicitly modeled in the simulations, their impact on the trajectories of the heavier atoms is negligible due to their significantly lower mass. Consequently, for the purposes of this analysis, the effects of hydrogen atoms are omitted, as they do not substantially influence the trajectories of the sulfur atoms.

**Results and discussion.** – Figure 2 illustrates the area covered by the 75th percentiles of the distribution of sulfur coordinates reaching the detector plane, as a function of the ion depths in the water slab and the beam parameters. The second  $y$ -axis in the same plot depicts the correspondence between the measured areas and the portion of the solid angle spanned by them.

Firstly, we examine simulations conducted at 8 keV. In fig. 2 we see that the spread in the sulfur ion trajectories does not seem to depend very strongly on the depth. The spread in the area is about the same for a sulfur that originates from a position 14 Å from the surface, as for a sulfur located right at the surface. At this photon energy and intensity, the final charge of S and O are rather similar, as seen in table 1. There are two forces acting on the sulfur ion, the force caused by the van der Waals potential, and the hybrid screened Coulomb force. In the situation where the system is highly charged, the Coulomb force is

Table 1: Simulation averaged charge of oxygen and sulfur for the two pulse parameters explored, as given by the CR simulations.

Intensity, energy	Oxygen charge	Sulfur charge
$10^{18} \text{ Wcm}^{-2}$ , 2 keV	5.17	8.63
$6 \times 10^{18} \text{ Wcm}^{-2}$ , 8 keV	1.69	1.40

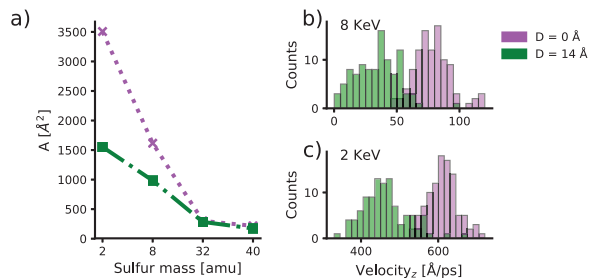


Fig. 3: Panel (a): area covered by the 75th percentiles of the point distribution of the projections of the ion explosions as a function of the ion mass. Panels (b) and (c): distribution for the  $Z$ -component of velocity for ions with native sulfur mass, starting at depth 0 Å and 14 Å. The photon energy is 8 keV for panel (b) and 2 keV for panel (c).

the main accelerator. The magnitude of the acceleration depends on the force and the mass of the particle being accelerated. In the approximation that we can consider each ion-ion interaction separately, the force is governed by the charges on the particles,  $F_{\text{Coulomb}} \sim q_1 q_2$ . Under the assumption that the hydrogens are too light to have any effect on the acceleration of sulfur or oxygen, we can conclude that the force the sulfur experiences is related to the sulfur charge times the oxygen charge,  $F_{\text{Coulomb}} \sim q_S q_O$ , and the force the average oxygen experiences is  $F_{\text{Coulomb}} \sim q_O q_O$ . In the 8 keV simulations,  $q_O^{8\text{keV}} q_S^{8\text{keV}} = 2.89e^2$ , and  $q_O^{8\text{keV}} q_S^{8\text{keV}} = 2.38e^2$ , therefore the forces that oxygen and sulfur are experiencing do not differ much. The mass of oxygen is half the mass of sulfur, and hence the acceleration due to the Coulomb force on the sulfur is only half compared to what the oxygen is experiencing. The dynamics of the sulfur atom will therefore be slower than the oxygen atoms. Even when the sulfur atom is close to the surface, it will not have enough time to propagate into vacuum, before the oxygen atoms have overtaken it. This makes the environment that the sulfur sees and thus the Coulomb forces that it experiences, independent of its initial the depth. The behavior can be well described with a hydrodynamics expansion model, as was presented by Hau-Riege *et al.* [32]

Due to the large difference in photoionization cross-section, the situation is different in the 2 keV case. Here  $q_O^{2\text{keV}} q_S^{2\text{keV}} = 45e^2$  and  $q_O^{2\text{keV}} q_O^{2\text{keV}} = 25e^2$ , but the masses are the same as in the 8 keV simulations (ignoring the mass of the electrons). With the force on the sulfur being about twice the force on the oxygen atoms, and the mass of the

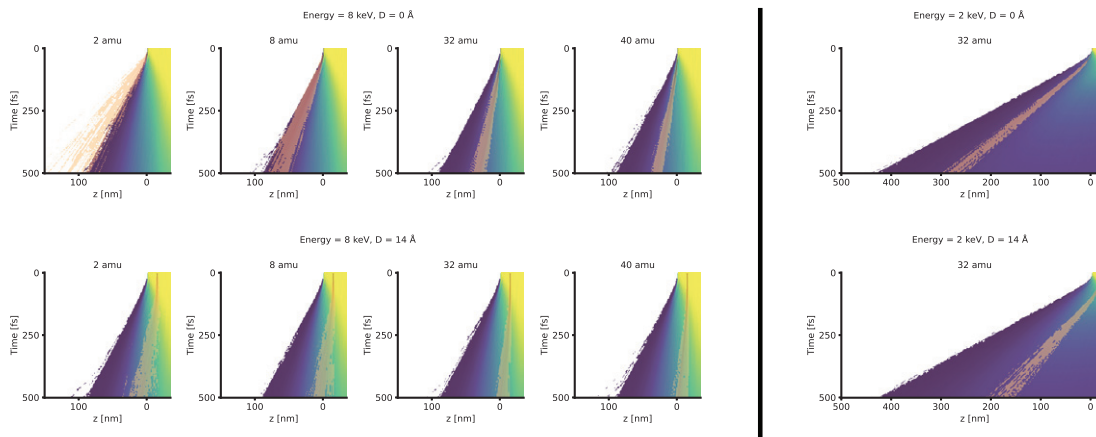


Fig. 4: Illustrations of the time-dependent expansion dynamics of oxygen and sulfur projected along the  $z$ -axis within the simulation box. The simulations depict the situation of sulfur ions at a depth of  $0 \text{ \AA}$  (top) and  $14 \text{ \AA}$  (bottom) from the water/vacuum interface (the value of  $z = 0$  on the  $x$ -axis corresponds to the water surface). For the case at  $8 \text{ keV}$ , arranged from left to right, the plots correspond to the four scenarios with S mass set at  $40 \text{ amu}$ ,  $32 \text{ amu}$ ,  $8 \text{ amu}$ , and  $2 \text{ amu}$ . In each plot, the collective information derived from 100 independent simulations shows the averaged trends observed at every time step.

sulfur being twice the mass of the oxygen, we therefore end up in a situation where the two ion types are accelerated in a similar way. In this situation it seems like the individual Coulomb collisions play a more important role. In fig. 2, we can see that the spread of the sulfur ion trajectories depends on the depth. The deeper into the bulk the ions start, the more chances of collisions they have before the surrounding density gets too low. More collisions leads to more randomness in the trajectories and a larger difference between individual simulations, which in turn generates a larger spread. This behaviour is better described by the Coulomb interaction (or Coulomb explosion [3,33,34]), than with hydrodynamic expansion as mentioned earlier. At  $14 \text{ \AA}$  depth the spread seems to decrease again and a possible explanation for this is that our limited set of 100 simulations per depth causes fluctuations in the data point. Simulations at a depth of  $16 \text{ \AA}$ , not shown, indicate an increase.

To validate the above reasoning, we conducted a simple test to study the relationship between the acceleration of oxygen atoms and sulfur. To do so, we altered the mass of the sulfur in a new set of simulations conducted at  $8 \text{ keV}$  photon energy. The mass of the sulfur-like particle was systematically varied from  $32 \text{ amu}$  to  $40 \text{ amu}$ ,  $8 \text{ amu}$ , and  $2 \text{ amu}$ , while keeping other simulation parameters consistent with those used in the previous simulations. Not unexpectedly, this mass adjustment resulted in a change in acceleration of the sulfur-like particle, particularly in comparison to the oxygen atoms. With increased acceleration for the lighter  $8 \text{ amu}$  and  $2 \text{ amu}$  cases, and a decrease for the  $40 \text{ amu}$  case. Results of these simulations, limited to depths of  $0 \text{ \AA}$  and  $14 \text{ \AA}$ , are depicted in panel a of fig. 3. The figure shows the area covered by the 75th percentiles of the ion explosion projections as a function of ion mass, indicating that lighter particles have a broader spread. Changing the sulfur-like particle to

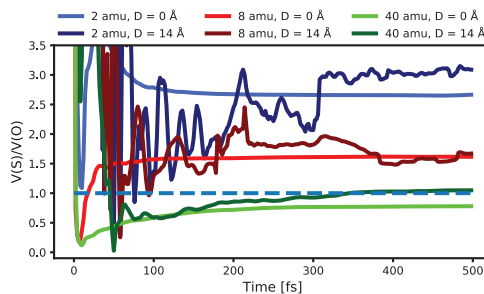


Fig. 5: Ratio of the ion velocity to mean velocity of surrounding oxygen for different sulfur-like ion mass. We take the group velocity of all the atoms starting within  $\pm 1 \text{ \AA}$  of the ion, averaged over all simulations, and for the ion it is simply the average velocity over all simulations.

$40 \text{ amu}$  showed a negligible impact on spread compared to  $32 \text{ amu}$  atoms. Same results are visible in fig. 4, where the average densities of water over time, overlaid by individual sulfur-like particle trajectories from the 100 simulations, are presented. These observations lead to two conclusions: firstly, the spread is wider with lighter particles, and secondly, lighter particles travel further on average, as expected given the mass-dependent trajectory. The lighter the sulfur-like particles are, the more influenced by the hydrogens they are, and the more they behave like hydrogens. Sulfur-like particles with a mass of  $2 \text{ amu}$  are ejected from the surface in the same manner as the hydrogens.

In fig. 5, we extend this analysis by comparing the velocities in the  $z$ -direction for sulfur-like particles and their adjacent oxygen atoms. By plotting the ratio of the average ion velocity to the average velocity of oxygen starting at the same depth, we can examine the expansion speed. Lighter ions consistently exhibit higher velocities than heavier ones, yet the velocity ratio between the ion and

oxygen remains fairly constant across different depths. At greater depths, ions show more erratic movement due to increased collision frequencies, a trend more pronounced in lighter ions. However, it is important to note that while the absolute speed decreases for both the ion and oxygen at greater depths, the average movement ratio relative to surrounding oxygen is maintained.

Building on these observations, the velocity-depth dependence could be a useful tool in estimating the depths of measured ions. This aligns with findings done with other simulations models, where the velocities of material at the surface have been shown to be greater than that in bulk [35]. The same trend is observed with sulfur-like ions, where the velocity distribution is significantly depth-dependent. An example of this effect is given in fig. 3 for the case of standard-mass sulfur ions, at 8 keV in panel (b) and 2 keV in panel (c) and for depths of  $D = 0 \text{ \AA}$  and  $D = 14 \text{ \AA}$ , where it is evident that the different depths yield to distinguishable velocity spread.

We hypothesize that with a detector capable of accurate momentum measurements, it would be possible to infer the depth of an ion. Such a capability would be invaluable in determining orientations in protein imaging experiments.

**Conclusions.** – In this study we have employed a hybrid CR/MD model to simulate photon-matter interaction of a sulfur atom in bulk water with a specific emphasis on analyzing ion trajectories induced by an XFEL pulse. Our investigation focused into the behavior of the sulfur atom’s trajectory, examining its dispersion as a function of initial depth to mimic potential scenarios involving heavy atoms positioned at different locations within a protein’s 3D structure. Depending on the pulse parameters used, and thus the relative charge states of the oxygen atoms and sulfur, different dependencies with depth were revealed. Using pulse parameters which induce a smaller force on the sulfur compared to oxygen, the dynamics of the sulfur were found to be independent of its depth. Conversely, under the condition of similar forces, the sulfur atom has a larger spread with increasing depth. In this latter case, artificially reducing the sulfur mass, would result in more chaotic expansion leading to even larger trajectory spreads. Our observations suggest the possibility of optimizing pulse parameters and the introduction of heavy atoms to a protein, similarly to current practices in serial femtosecond crystallography, to achieve reproducible ion trajectories. For the case of small molecules, the tracking of ion momenta distributions and positions during Coulomb exploding samples has been recently experimentally realized to provide valuable insights into their complex chemical dynamics [36–39]. Other experiments have demonstrated the capability of the Coulomb explosion imaging to probe orientation and alignment of the samples [40–42]. The solid angle spreads analyzed in our study are well within the capabilities of current state-of-the-art experimental technology at XFEL sources. Therefore, we

propose extending this approach to retrieve particle orientation during X-ray exposure in SPI experiments, aiming to enhance our understanding of biological systems.

\*\*\*

The authors thank Dr. ERIK MARKLUND for useful discussions. This work was supported by the innovation programme under grant agreement No. 801406 and SPIDoc’s within Marie Skłodowska Curie Action program HORIZON-MSCA-2022-DN Grant Agreement No. 101120312. EDS and CC acknowledge support from a Röntgen Ångström Cluster grant provided by the Swedish Research Council and the Bundesministerium für Bildung und Forschung (2021-05988) and by Project grants from the Swedish Research Council (2018-00740). CC further acknowledges the Helmholtz Association through the Center for Free-Electron Laser Science at DESY for financial support. The computations were enabled by resources provided by the National Academic Infrastructure for Supercomputing in Sweden (NAISS) and the Swedish National Infrastructure for Computing (SNIC) at Uppsala Multidisciplinary Center for Advanced Computational Science (UPPMAX) partially funded by the Swedish Research Council and by the daVinci computer cluster hosted at the laboratory of molecular biophysics.

*Data availability statement:* The data that support the findings of this study are available upon reasonable request from the authors.

## REFERENCES

- [1] BERMAN H. M., WESTBROOK J., FENG Z., GILLILAND G., BHAT T. N., WEISSIG H., SHINDYALOV I. N. and BOURNE P. E., *Nucleic Acids Res.*, **28** (2000) 235.
- [2] HOLTON J. M., *J. Synchrotron Radiat.*, **16** (2009) 133.
- [3] NEUTZE R., WOUTS R., VAN DER SPOEL D., WECKERT E. and HAJDU J., *Nature*, **406** (2000) 752.
- [4] SEIBERT M. M., EKEBERG T., MAIA F. R., SVENDA M., ANDREASSON J., JÖNSSON O., ODIĆ D., IWAN B., ROCKER A., WESTPHAL D. *et al.*, *Nature*, **470** (2011) 78.
- [5] LOH N.-T. D. and ELSER V., *Phys. Rev. E*, **80** (2009) 026705.
- [6] AYYER K., LAN T.-Y., ELSER V. and LOH N. D., *J. Appl. Crystallogr.*, **49** (2016) 1320.
- [7] MARKLUND E. G., EKEBERG T., MOOG M., BENESCH J. L. P. and CALEMAN C., *J. Phys. Chem. Lett.*, **8** (2017) 4540.
- [8] WOLLTER A., DE SANTIS E., EKEBERG T., MARKLUND E. G. and CALEMAN C., *J. Chem. Phys.*, **160** (2024) 114108.
- [9] KIERSPEL T., KADEK A., BARRAN P., BELLINA B., BIJEDIC A., BRODMERKEL M. N., COMMANDEUR J., CALEMAN C., DAMJANOVIĆ T., DAWOD I., DE SANTIS E., LEKKAS A., LORENZEN K., MORILLO L. L., MANDL T., MARKLUND E. G., PAPANASTASIOU D., RAMAKERS L. A.

- I., SCHWEIKHARD L., SIMKE F., SINELNIKOVA A., SMYRNAKIS A., TIMNEANU N., UETRECHT C. for the MS SPIDOC CONSORTIUM, *Anal. Bioanal. Chem.*, **415** (2023) 4209.
- [10] SINELNIKOVA A., MANDL T., AGELI H., GRÄNÄS O., MARKLUND E. G., CALEMAN C. and DE SANTIS E., *Bio-phys. J.*, **120** (2021) 3709.
- [11] POPP D., LOH N. D., ZORGATI H., GHOSHDASTIDER U., LIOW L. T., IVANOVA M. I., LARSSON M., DEPONTE D. P., BEAN R., BEYERLEIN K. R., GATI C., OBERTHUER D., ARNLUND D., BRÄNDÉN G., BERNTSEN P., CASCIO D., CHAVAS L. M., CHEN J. P., DING K., FLECKENSTEIN H., GUMPRECHT L., HARIMOORTHY R., MOSSOU E., SAWAYA M. R., BREWSTER A. S., HATTNE J., SAUTER N. K., SEIBERT M., SEURING C., STELLATO F., TILP T., EISENBERG D. S., MESSERSCHMIDT M., WILLIAMS G. J., KOGLIN J. E., MAKOWSKI L., MILLANE R. P., FORSYTH T., BOUTET S., WHITE T. A., BARTY A., CHAPMAN H., CHEN S. L., LIANG M., NEUTZE R. and ROBINSON R. C., *Cytoskeleton*, **74** (2017) 472.
- [12] ÖSTLIN C., TIMNEANU N., JÖNSSON H. O., EKEBERG T., MARTIN A. V. and CALEMAN C., *Phys. Chem. Chem. Phys.*, **20** (2018) 12381.
- [13] VELANKAR S., VAN GINKEL G., ALHROUB Y., BATTLE G. M., BERRISFORD J. M., CONROY M. J., DANA J. M., GORE S. P., GUTMANAS A., HASLAM P. *et al.*, *Nucleic Acids Res.*, **44** (2016) D385.
- [14] BEYERLEIN K. R., JÖNSSON H. O., ALONSO-MORI R., AQUILA A., BAJT S., BARTY A., BEAN R., KOGLIN J. E., MESSERSCHMIDT M., RAGAZZON D., SOKARAS D., WILLIAMS G. J., HAU-RIEGE S., BOUTET S., CHAPMAN H. N., TIMNEANU N. and CALEMAN C., *Proc. Natl. Acad. Sci. U.S.A.*, **115** (2018) 5652.
- [15] PATRA K. K., ELIAH DAWOD I., MARTIN A. V., GREAVES T. L., PERSSON D., CALEMAN C. and TIMNEANU N., *J. Synchrotron Radiat.*, **28** (2021) 1296.
- [16] DAWOD I. *et al.*, *ACS Phys. Chem. Au*, **4** (2024) 385.
- [17] DAWOD I. *et al.*, *J. Chem. Phys.*, **160** (2024) 184112.
- [18] SCOTT H. A. and MAYLE R. W., *Appl. Phys. B.*, **58** (1994) 35.
- [19] SCOTT H. A., *J. Quant. Spectrosc. Radiat. Transf.*, **71** (2001) 689.
- [20] HESS B., KUTZNER C., VAN DER SPOEL D. and LINDAHL E., *J. Chem. Theory Comput.*, **4** (2008) 435.
- [21] MURILLO M. S. and WEISHEIT J. C., *Phys. Rep.*, **302** (1998) 1.
- [22] MORSE P. M., *Phys. Rev.*, **34** (1929) 57.
- [23] KOZLOV A., MARTIN A. V. and QUINEY H. M., *Crystals*, **10** (2020) 478.
- [24] NASS K., GOREL A., ABDULLAH M., MARTIN A., KLOOS M., MARINELLI A., AQUILA A., BARENDT S., DECKER F.-J., DOAK R., FOUCAR L., HARTMANN E., HILPERT M., HUNTER M., JUREK Z., KOGLIN J., KOZLOV A., LUTMAN A., KOVACS G. and SCHLICHTING I., *Nat. Commun.*, **11** (2020) 1814.
- [25] BUSSI G., DONADIO D. and PARRINELLO M., *J. Chem. Phys.*, **126** (2007) 014101.
- [26] BERENDSEN H. J., POSTMA J. V., VAN GUNSTEREN W. F., DiNOLA A. and HAAK J. R., *J. Chem. Phys.*, **81** (1984) 3684.
- [27] JORGENSEN W. L., CHANDRASEKHAR J., MADURA J. D., IMPEY R. W. and KLEIN M. L., *J. Chem. Phys.*, **79** (1983) 926.
- [28] MACKERELL A. D. jr., BASHFORD D., BELLOTT M., DUNBRACK R. L. jr., EVANSECK J. D., FIELD M. J., FISCHER S., GAO J., GUO H., HA S., JOSEPH-McCARTHY D., KUCHNIR L., KUCZERA K., LAU F. T. K., MATOS C., MICHNICK S., NGO T., NGUYEN D. T., PRODHOM B., REIHER W. E. III, ROUX B., SCHLENKRICH M., SMITH J. C., STOTE R., STRAUB J., WATANABE M., WIÓRKIEWICZ-KUCZERA J., YIN D. and KARPLUS M., *J. Phys. Chem. B.*, **102** (1998) 3586.
- [29] DARDEN T., YORK D. and PEDERSEN L., *J. Chem. Phys.*, **98** (1993) 10089.
- [30] WASKOM M. L., *J. Open Source Softw.*, **6** (2021) 3021.
- [31] BRADEN B., *Coll. Math. J.*, **17** (1986) 326.
- [32] HAU-RIEGE S., LONDON R., HULDT G. and CHAPMAN H., *Phys. Rev. E*, **71** (2005) 061919.
- [33] JUREK Z., OSZLÁNYI G. and FAIGEL G., *Europhys. Lett.*, **65** (2004) 491.
- [34] BERGH M., TIMNEANU N. and VAN DER SPOEL D., *Phys. Rev. E*, **70** (2004) 051904.
- [35] HAU-RIEGE S. P., LONDON R. A. and SZOKE A., *Phys. Rev. E*, **69** (2004) 051906.
- [36] BOLL R., SCHÄFER J. M., RICHARD B., FEHRE K., KASTIRKE G., JUREK Z., SCHÖFFLER M. S., ABDULLAH M. M., ANDERS N., BAUMANN T. M. *et al.*, *Nat. Phys.*, **18** (2022) 423.
- [37] BHATTACHARYYA S., BORNE K., ZIAEE F., PATHAK S., WANG E., VENKATACHALAM A. S., LI X., MARSHALL N., CARNES K. D., FEHRENBACH C. W. *et al.*, *J. Phys. Chem. Lett.*, **13** (2022) 5845.
- [38] LI X., RUDENKO A., SCHÖFFLER M., ANDERS N., BAUMANN T. M., ECKART S., ERK B., DE FANIS A., FEHRE K., DÖRNER R. *et al.*, *Phys. Rev. Res.*, **4** (2022) 013029.
- [39] CHENG C., FRASINSKI L. J., MOĞOL G., ALLUM F., HOWARD A. J., ROLLES D., BUCKSBAUM P. H., BROUARD M., FORBES R. and WEINACHT T., *Phys. Rev. Lett.*, **130** (2023) 093001.
- [40] AMINI K., BOLL R., LAUER A., BURT M., LEE J. W., CHRISTENSEN L., BRAUßE F., MULLINS T., SAVELYEV E., ABLIKIM U. *et al.*, *J. Chem. Phys.*, **147** (2017) 013933.
- [41] VALLANCE C., HEATHCOTE D. and LEE J. W., *J. Phys. Chem. A*, **125** (2021) 1117.
- [42] CHATTERLEY A. S., SHEPPERSON B. and STAPELFELDT H., *Phys. Rev. Lett.*, **119** (2017) 073202.